

1 **Deep Dive into Hydrologic Simulations at Global Scale: Harnessing the Power of Deep** 2 **Learning and Physics-informed Differentiable Models (δ HBV-globe1.0-hydroDL)**

3 Dapeng Feng^{1,2,3}, Hylke Beck⁴, Jens de Bruijn^{3,5}, Reetik Kumar Sahu³, Yusuke Satoh⁶, Yoshihide Wada⁷,
4 Jiangtao Liu¹, Ming Pan⁸, Kathryn Lawson¹, Chaopeng Shen^{1*}

5
6 ¹ Civil and Environmental Engineering, Pennsylvania State University, University Park, PA, USA

7 ² Earth System Science, Stanford University, Stanford, CA, USA

8 ³ Water Security Research Group, International Institute for Applied Systems Analysis (IIASA), Laxenburg, Austria

9 ⁴ Climate and Livability Initiative, Physical Science and Engineering Division, King Abdullah University of Science and
10 Technology, Thuwal, Saudi Arabia

11 ⁵ Institute for Environmental Studies (IVM), Vrije Universiteit Amsterdam, Amsterdam, Netherlands

12 ⁶ Moon Soul Graduate School of Future Strategy, Korea Advanced Institute of Science and Technology, Daejeon, Republic of
13 Korea

14 ⁷ Climate and Livability Initiative, Center for Desert Agriculture, Biological and Environmental Science and Engineering
15 Division, King Abdullah University of Science and Technology, Thuwal, Saudi Arabia

16 ⁸ Center for Western Weather and Water Extremes, Scripps Institution of Oceanography, University of California San Diego,
17 La Jolla, CA, USA

18 *Correspondence to: Chaopeng Shen (cshen@enr.psu.edu)

19 **Abstract.** Accurate hydrological modeling is vital to characterizing how the terrestrial water cycle responds to climate change.
20 Pure deep learning (DL) models have shown to outperform process-based ones while remaining difficult to interpret. More
21 recently, differentiable, physics-informed machine learning models with a physical backbone can systematically integrate
22 physical equations and DL, predicting untrained variables and processes with high performance. However, it was unclear if
23 such models are competitive for global-scale applications with a simple backbone. Therefore, we use - for the first time at this
24 scale - differentiable hydrologic models (full name δ HBV-globe1.0-hydroDL, shortened to δ HBV here) to simulate the
25 rainfall-runoff processes for 3753 basins around the world. Moreover, we compare the δ HBV models to a purely data-driven
26 long short-term memory (LSTM) model to examine their strengths and limitations. Both LSTM and the δ HBV models provide
27 competent daily hydrologic simulation capabilities in global basins, with median Kling-Gupta efficiency values close to or
28 higher than 0.7 (and 0.78 with LSTM for a subset of 1675 basins with long-term records), significantly outperforming
29 traditional models. Moreover, regionalized differentiable models demonstrated stronger spatial generalization ability (median
30 KGE 0.64) than a traditional parameter regionalization approach (median KGE 0.46) and even LSTM for ungauged region
31 tests in Europe and South America. Nevertheless, relative to LSTM, the differentiable model was hampered by structural

32 deficiencies for cold or polar regions, and highly arid regions, and basins with significant human impacts. This study also sets
33 the benchmark for hydrologic estimates around the world and builds foundations for improving global hydrologic simulations.

34

35 **Short Summary.** Accurate hydrologic modeling is vital to characterizing water cycle responses to climate change. For the
36 first time at this scale, we use differentiable physics-informed machine learning hydrologic models to simulate rainfall-runoff
37 processes for 3753 basins around the world and compare them with purely data-driven and traditional approaches. This sets a
38 benchmark for hydrologic estimates around the world and builds foundations for improving global hydrologic simulations.

39

40 **Key Words.** Physics-informed machine learning; Differentiable hydrologic models; Global hydrologic modeling; high
41 resolution evaluation; Parameter regionalization; Prediction in ungauged regions

42 1. Introduction

43 Hydrological models are vital tools to model and elucidate the terrestrial water cycle, and have been widely used in flood
44 forecasting (Maidment, 2017), water resources management (Jayakrishnan et al., 2005), and assessing climate change impacts
45 (Hagemann et al., 2013). Recently, deep learning (DL) models have demonstrated superior performance compared to
46 traditional process-based hydrological models in accurately predicting different components of the hydrologic cycle (Shen,
47 2018), such as soil moisture (Fang et al., 2017, 2019; Fang and Shen, 2020), streamflow (Feng et al., 2020; Konapala et al.,
48 2020; Kratzert et al., 2019b; Liu et al., 2024), snow water equivalent (Cui et al., 2023; Song et al., 2024), groundwater (Wunsch
49 et al., 2021) and water quality (Hansen et al., 2022; Rahmani et al., 2021; Saha et al., 2023; Zhi et al., 2021; Chaemchuen et
50 al., 2023). Long short-term memory (LSTM) networks, which are a type of recurrent neural network (Hochreiter and
51 Schmidhuber, 1997), and **Transformers** are currently popular DL algorithms for handling time series dynamics in hydrology,
52 while other architectures like transformers can also be employed. LSTM models have established state-of-the-art accuracy for
53 streamflow prediction at continental and smaller scales (Feng et al., 2020, 2021; Kratzert et al., 2019a, b; Lees et al., 2021;
54 Mai et al., 2022).

55

56 Although DL models have shown great prediction accuracy compared to traditional models, they usually do not possess clear
57 physical constraints inside the model and are often considered to be “black boxes”, despite recent efforts shed by some
58 interpretive efforts (Lees et al., 2022). Thus, purely data-driven models are limited in that they cannot predict unobservable or
59 untrained physical variables, and impede the investigation of the physical relations of different hydrologic variables behind
60 the change in the target variable. They may also become overfitted and acquire incorrect sensitivities to inputs (Reichert et al.,
61 2024). In contrast, traditional process-based hydrologic models following physical laws like mass balances can provide a full
62 set of diagnostic outputs for hydrologic variables like soil water storage, groundwater recharge, evapotranspiration and snow
63 water equivalent, even though they are usually only calibrated on discharge observations (Burek et al., 2020; Müller Schmied

64 et al., 2014). The multivariate output nature of these models provides an opportunity for calibration on one or more observable
65 variables to better predict other, perhaps unobservable, variables (in reality, whether this is the case or not depends on if the
66 issue of parameter non-uniqueness is addressed). However, it seems quite difficult for the traditional physical model to
67 approach the performance level of the DL models in daily hydrograph metrics (Feng et al., 2020; Kratzert et al., 2019b) or to
68 improve in generalization with increasing training data (Tsai et al., 2021). In addition, traditional calibration is typically done
69 site-by-site and can be time- and labor-intensive. Therefore, it logically follows that integrating DL and process-based models
70 might enable harnessing their respective strengths while circumventing their weaknesses (Shen et al., 2023).

71

72 By combining a physical model with a DL model, differentiable modeling (Shen et al., 2023) provides a systematic solution
73 to leveraging the strengths of both model types while circumventing their limitations. In differentiable models, we use process-
74 based models as a backbone and insert neural networks to either provide parameters (Tsai et al., 2021) or process substitutes
75 for physical models (Aboelyazeed et al., 2023; Feng et al., 2022, 2023; Höge et al., 2022; Jiang et al., 2020), or they could use
76 limited physical constraints (Kraft et al., 2022). They are collectively called “differentiable models” in the sense that they can
77 rapidly compute gradients of outputs with respect to inputs or parameters using automatic differentiation (or any other means).
78 The differentiability enables the training of neural network components placed anywhere in the model via backpropagation.
79 Inserting neural networks into process-based models can be perceived as posing questions regarding some uncertain
80 relationships given some known ones (priors) and we want to get answers for these questions by automatically learning from
81 big data.

82

83 Some of our recent work has applied differentiable modeling to the conceptual hydrologic model named Hydrologiska Byråns
84 Vattenbalansavdelning (HBV) (Bergström, 1976, 1992; Seibert and Vis, 2012), and built a physics-informed hybrid model for
85 basins in the contiguous United States (CONUS) (Feng et al., 2022, 2023). The model is “regionalized” in the sense that the
86 embedded neural network components are trained simultaneously on all basins in the study region in order to provide physical
87 HBV parameters which are learned from raw information of basin attributes, resulting in improved generalizability and reduced
88 overfitting to local noise. With the help of differentiable modeling to flexibly evolve the original structure of HBV, the
89 differentiable hybrid models can approach the performance level of the LSTM model, whilst being constrained to physical
90 laws and keeping process clarity to predict untrained diagnostic variables with decent accuracy (Feng et al., 2022). Since the
91 framework is regionalized, this differentiable model can be used to predict in ungauged regions and even extrapolates better
92 spatially than LSTM in data-sparse regions when tested across the CONUS (Feng et al., 2023).

93

94 Owing to the complexity of calibration, current global hydrologic models are largely either uncalibrated (Hattermann et al.,
95 2017; Zaherpour et al., 2018) or only calibrated on mean annual water budgets or in limited regions (Burek et al., 2020; Müller
96 Schmied et al., 2014). Only very limited studies attempt to calibrate global models on monthly discharge variations (Werth
97 and Güntner, 2010). We desire efficient regionalized models that maximally leverage available information and provide

98 accurate predictions to diverse basins across different climate groups and geographic characteristics in the world. We also want
99 the models to perform decently even in data-sparse regions, showing competitive extrapolation ability, given that many large
100 regions such as in Africa and Asia lack publicly available streamflow data. DL and differentiable models seem plausible
101 candidates for such simulations. Nevertheless, previous studies on DL and physics-informed differentiable models mainly
102 focus on continental or smaller scales, with a relatively homogeneous forcing dataset --- it is unclear if their observed strengths,
103 e.g., high performance and strong generalization ability, can carry over to global scales, where the climate is much more diverse
104 and datasets differ widely in their biases and uncertainty characteristics. In particular, we want to thoroughly examine how
105 well these models can leverage information learned in data-rich continents to characterize the hydrologic processes in
106 ungauged regions across the world. Meanwhile, DL models also show favorable scaling relationships (or data synergy) where
107 more data leads to more robust models (Fang et al., 2022). Thus, training on a larger dataset may provide additional benefits.

108

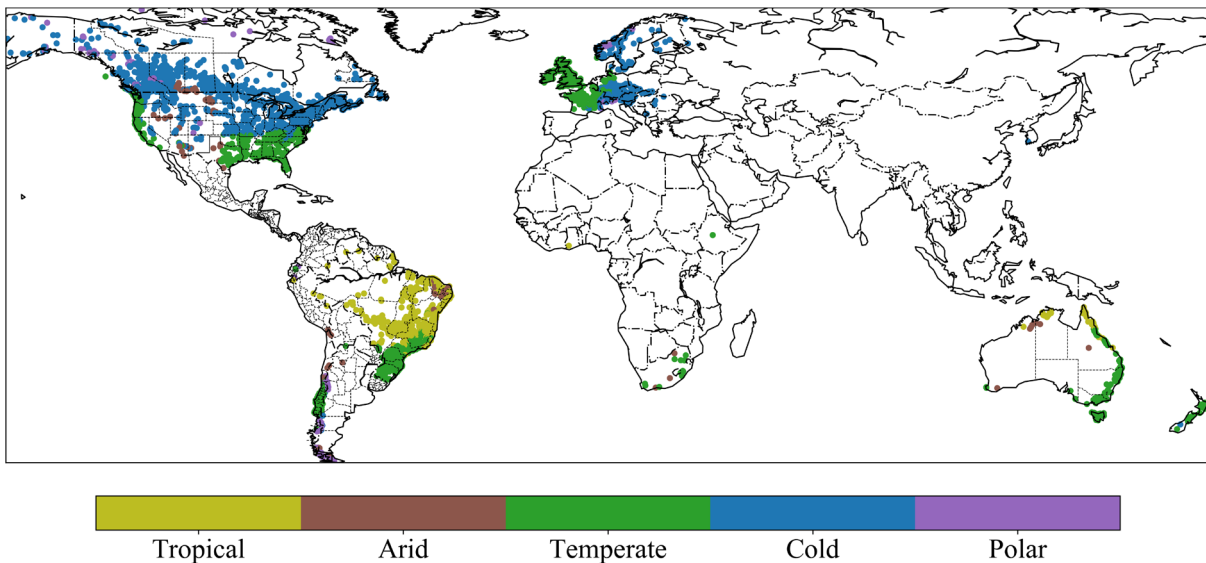
109 In this study, we test physics-informed differentiable models (with the full version name δ HBV-globe1.0-hydroDL, where “ δ ”
110 represents “differentiable”, globe1.0 is the version, and “hydroDL” refers to our particular code implementation. δ HBV is
111 used as the abbreviation in this paper) to simulate hydrologic processes for global basins and compare results to purely data
112 driven methods and traditional modeling approach. We focus on regionalized modeling and emphasize the importance of
113 spatial generalization in data-sparse scenarios, since observed streamflow data in many parts of the world are scarce. This
114 means one framework with parameter regionalization from geographic attributes will be used to model all the global basins
115 rather than calibrating a separate model in each individual basin (Beck et al., 2020b; Feng et al., 2022; Mizukami et al., 2017).
116 We first investigate what prediction accuracy can be achieved by different models at global scale by learning from a large and
117 diverse dataset. We then relate the global spatial patterns of model performance to geographic characteristics and hydrologic
118 processes to identify model structural deficiencies and gain hydrologic insights. Finally, we provide evidence indicating which
119 type of model may be more appropriate for next-generation global modeling by rigorously examining their generalizability to
120 ungauged regions across the world.

121 **2. Data and methods**

122 **2.1 Global datasets**

123 We use a global database compiled in a previous study (Beck et al., 2020b) which contains a total of 4229 headwater
124 catchments. The dataset includes basin mean meteorological forcings, catchment characteristics such as the climate,
125 topography, land cover, soil composition, and geology information to support parameter regionalization, along with streamflow
126 gauge discharge observations. Meteorological forcings are the driving inputs of hydrological models. This global dataset
127 includes daily precipitation from Multi-Source Weighted-Ensemble Precipitation (MSWEP), a product that merges gauge,
128 satellite, and reanalysis precipitation data (Beck et al., 2017c, 2019), and maximum and minimum temperature from Multi-
129 Source Weather (MSWX), a product that bias-corrects and harmonizes meteorological data from atmospheric reanalyses and

130 weather forecast models (Beck et al., 2022). Potential evapotranspiration was estimated using the method from Hargreaves
131 (1994). The discharge observations at the outlet gauges were used as prediction targets to train the hydrologic models. We
132 excluded some basins with potential erroneous discharge records such as showing unreasonable magnitude way larger than
133 precipitation or dramatic differences between two time intervals, by manually performing visual screening, and also excluded
134 those with severe amounts of missing data (less than 5 years' worth of data points in the study period from 2000 to 2016).
135 Thus, 3753 basins were finally used to evaluate different models. These basins had been classified into five Köppen-Geiger
136 climate classes in Beck et al., (2020b), including tropical (489 basins), arid (109 basins), temperate (1423 basins), cold (1593
137 basins), and polar (139 basins), as shown in Figure 1. To evaluate the simulations of untrained variables like evapotranspiration
138 (ET), the MOD16A2GF (Running et al., 2021), a gap-filled 8-day composite ET product estimated from the Moderate
139 Resolution Imaging Spectroradiometer (MODIS) satellite data and meteorological reanalysis data, were used as independent
140 observations to compare against the simulated ET from differentiable hydrologic models.

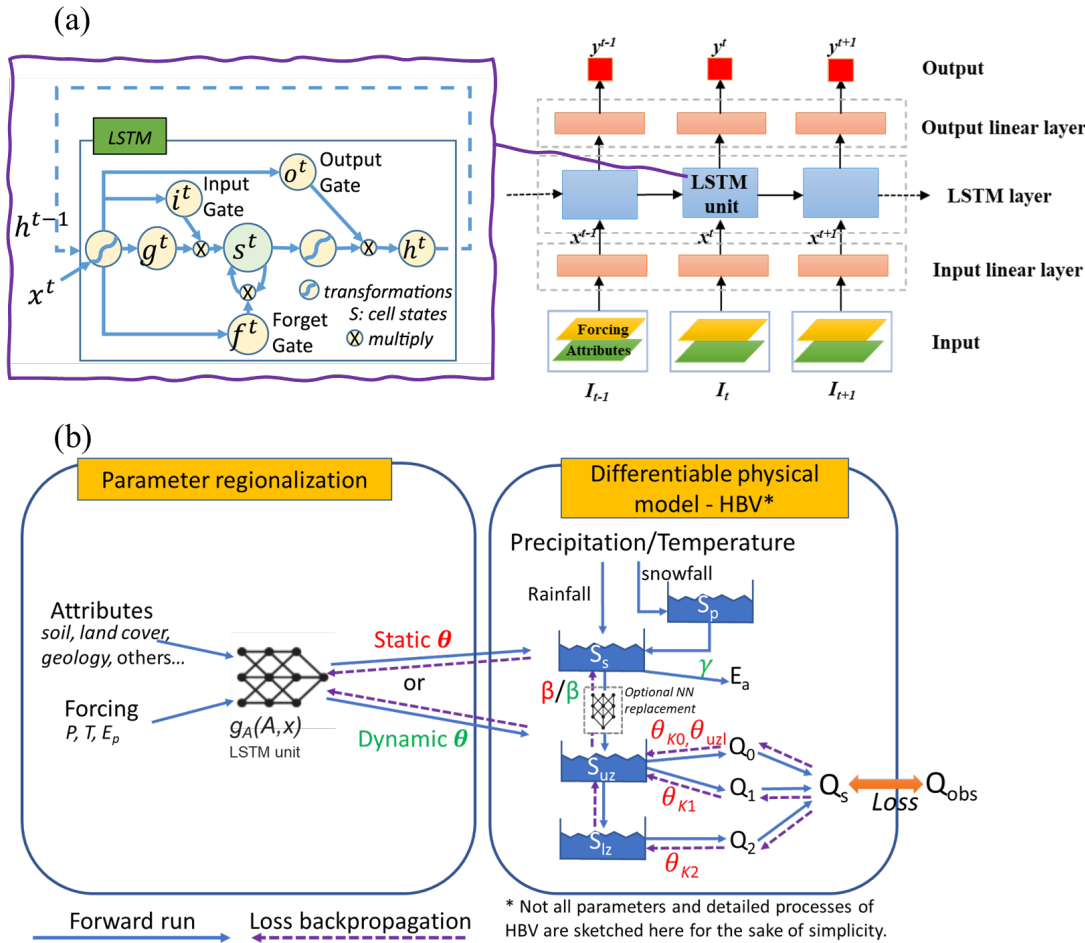


141
142 *Figure 1. Locations and climate groups of the 3753 global basins used in this study, which were originally compiled by Beck et al., 2020.*
143 *Plotted in Python using Matplotlib Basemap Toolkit.*

144 2.2 The long short-term memory (LSTM) streamflow model for comparison

145 Here the LSTM model is used as a benchmark for purely data-driven DL. The LSTM has “cell states” and “gates” to maintain
146 and filter information, as shown in Figure 2a. The input, forget, and output gates control the flow of information, respectively
147 controlling what to let in, what to forget, and what to output from the system. In this study we use the LSTM streamflow model
148 demonstrated in Feng et al. (2020) which has been successfully applied to simulate streamflow in hundreds of basins across
149 the CONUS. The framework takes meteorological forcings and basin attributes as inputs and generates daily streamflow
150 predictions for each basin at each time step (Figure 2a). We used mini-batches to train the LSTM model, where each minibatch

151 was composed of two-year sequences from 256 randomly-selected basins. The first-year sequences are only used for
 152 initializing the cell states, so we calculate the batch loss function only on the second-year sequences. The training sequences
 153 were also randomly selected from the whole training period, and one epoch was finished when the model had seen all the
 154 training data. Note that this sequence length is a subset of, and different concept from, the length of training period. Sequence
 155 length specifically refers to the length of the training instance that comprises a minibatch, whereas training period refers to the
 156 whole period when observations are available for training, from which the minibatch sequence length is randomly selected.
 157 The model was forwarded on each minibatch iteratively and its weights were updated using gradient descent after each
 158 forwarding. One epoch was considered to have occurred when the model is iterated over all the training data. We trained the
 159 LSTM model for 300 epochs to achieve convergence.



160

161 **Figure 2. Illustrations of two different types of regionalized hydrologic models. (a) Framework of the purely data-driven LSTM**
 162 **streamflow model (adapted from Figure 2 in Feng et al., 2020), and (b) framework of the differentiable HBV model (δ HBV-globe1.0-**
 163 **hydroDL) with parameter regionalization developed in Feng et al. (2022) (adapted from Figure 1 in Feng et al. (2022)). The neural**
 164 **network g_A here is a LSTM unit which is trained by the observed streamflow to produce the static or dynamic physical HBV parameters**
 165 **(θ, β, γ) from basin characteristics.**

166 2.3 The hybrid differentiable hydrologic models

167 We used the hybrid differentiable models (δ HBV-globe1.0-hydroDL) developed in Feng et al., (2022) for regionalized
168 modeling in global basins. The HBV model used here as the physical backbone is a conceptual hydrologic model with
169 representations of snowpack, soil, and groundwater storages, and can simulate flux variables such as snow melting,
170 evapotranspiration, and quick and slow outflows (Beck et al., 2020b; Bergström, 1976, 1992; Seibert and Vis, 2012). The
171 differentiable parameter learning (dPL) framework (Tsai et al., 2021) is used to provide parameter regionalization for HBV,
172 as shown by the g_A neural network in Figure 2b. The g_A network, which is a LSTM unit here, takes basin attributes and
173 meteorological forcings as inputs, and outputs static or dynamic physical HBV parameters. The differentiable HBV model
174 then takes these parameters as well as the meteorological forcings to simulate the hydrological process and predict daily
175 streamflow discharge along with other key flux variables. The whole framework including HBV itself was implemented in a
176 DL platform (PyTorch 1.0.1 was used for the original development and the model has also shown good compatibility with
177 more recent PyTorch versions, (Paszke et al., 2017)) supporting automatic differentiation and trained with gradient descent to
178 minimize the difference between the simulated and observed streamflow (the loss function). As in Feng et al., (2022), we
179 employed the loss function based on root-mean-square error (RMSE) with two weighted parts. The first part calculates RMSE
180 directly on the simulated and observed discharge, while the second part calculates RMSE on the transformed discharge records
181 to improve low flow representations. Note that we do not directly train the HBV parameters; rather, we focus on training the
182 weights of the g_A neural network to map the relationship between basin-averaged characteristics and HBV parameters.
183 Differentiable models are also trained in mini-batches that are formed in the same way as for training the LSTM streamflow
184 model. Within one epoch, differentiable models are forwarded and optimized over the randomly formed mini-batches until the
185 iterations have used all the training data points. We train the differentiable models for 50 epochs in total.

186

187 As described in Feng et al. (2022), the differentiable modeling framework enables optional modification of the structures of
188 the original HBV model to enable better performance and we use two versions of evolved HBV models in this study. We used
189 16 parallel subbasin-scale response units, each with a separate set of parameters to describe a fraction of the basin with different
190 hydrologic responses. These components implicitly represent subbasin-scale spatial heterogeneity. The simulated fluxes (e.g.,
191 streamflow) are the average of all the response units. The parameters of the multiple components are different and all are
192 produced simultaneously by the same g_A network. The first version of our model (referred to as “dPL + evolved HBV”) only
193 has static parameters which are kept constant during the hydrologic simulation. The second version (referred to as “dPL +
194 evolved HBV with DP) further allows some formerly static parameters of the multi-component model to vary daily with the
195 meteorological forcings. These dynamic parameters (DP) were also produced by the g_A LSTM unit. If we were to apply the
196 dynamic parameterization to all parameters, the model could become overly flexible, potentially leading to overfitting to the
197 training data (which would lead to issues with extrapolation beyond the training data). To reduce the risk of overfitting, we
198 restricted the dynamism to only two empirical parameters: the shape coefficient β in the equation that describes the

199 relationships between soil storage and potential runoff, and a newly added shape parameter (γ) which is involved in the
200 calculation of evapotranspiration. For more details regarding these differentiable HBV models, please refer to our previous
201 studies (Feng et al., 2022, 2023).

202 **2.4 Experiments and evaluation metrics**

203 We ran one temporal and two spatial generalization experiments to evaluate the performance of different regionalized models.
204 For the temporal generalization experiment, the models were trained for the period of 2000 to 2016 on all global basins, and
205 tested for the period of 1980 to 1997. Basins without discharge records or with less than 5 years' worth of data points in the
206 testing period were excluded from the evaluation. Without spatially holding out any basin during training, this experiment
207 aimed at evaluating the model's generalizability in the time dimension by testing prediction ability on the same basins but in
208 a different time period from the training data. The other two spatial generalization experiments served as the true litmus tests
209 for evaluating the effectiveness of regionalization schemes, i.e., how well the model can be applied to basins that have never
210 been seen during training. The first spatial generalization experiment was a traditional "prediction in ungauged basins" (PUB)
211 problem, where we randomly divided the whole global basin set into 10 folds (groups) and performed cross-validation across
212 these folds to obtain spatial out-of-sample predictions for all basins (training on 9 of the folds with the 10th fold held out and
213 testing on the 10th, then rotating such that each fold is used for testing once). The second spatial generalization experiment,
214 which we refer to as cross-continent "prediction in ungauged regions" (PUR), was more challenging. In this experiment, we
215 assumed that all the basins in certain continents are ungauged and excluded from the training dataset, trained a regionalized
216 model in other data-rich continents, and then tested the trained model to make predictions in the ungauged continents. With
217 random hold-out, an ungauged test basin in the first spatial generalization experiment always has training gauges surrounding
218 it. Therefore, the first PUB experiment can be interpreted as spatial interpolation. The second spatial experiment (cross-
219 continent PUR) holds out all the basins in one continent as testing targets, and thus is the much harder test of spatial
220 extrapolation.

221
222 To evaluate the overall performance of the hydrologic models, we used the Kling-Gupta Efficiency (KGE) (Gupta et al., 2009;
223 Kling et al., 2012) as compared in Beck et al., (2020b) and Nash-Sutcliffe Efficiency (NSE) (Nash and Sutcliffe, 1970). KGE
224 has three components that account for correlation, mean bias, and variability bias, while NSE mainly represents the variance
225 explained by the simulations. Both metrics indicate better performance when their values are closer to the maximum value of
226 1. We also examined the percent bias of the top 2% peak flow range (FHV) and bottom 30% low flow range (FLV) of
227 streamflow predictions to evaluate the model's ability to simulate extreme events (Yilmaz et al., 2008). All the reported
228 performance metrics in this study are from model evaluation on the testing dataset, which is not seen by the model during the
229 training process.

230 **3. Results and discussions**

231 **3.1 General patterns over global basins**

232 From the standpoint of daily hydrograph metrics (KGE and NSE), LSTM and the two differentiable models all achieved highly
233 competitive performance for the global basins in the temporal test (trained and tested on the same basins, but in different time
234 periods) (Figure 3). For the global dataset, all three models obtained median KGE values close to or higher than 0.7, but the
235 LSTM model performed the best of the three models here, achieving a median NSE (KGE) value of 0.70 (0.74) for all the
236 evaluated basins. For a subset of 1675 basins with long-term records (at least 15 years' worth of streamflow data available in
237 the training period and 5 years' worth of data available in the testing period, though not necessarily continuous), LSTM even
238 reached a median KGE of 0.78 (see Figure A1). Both versions of the differentiable models approached the performance level
239 of the LSTM, in agreement with our previous assessment for the CONUS (Feng et al., 2022). The model with dynamic
240 parameters achieved a median NSE (KGE) of 0.67 (0.69), followed by the model with static parameters, which obtained a
241 median NSE (KGE) of 0.65 (0.68).

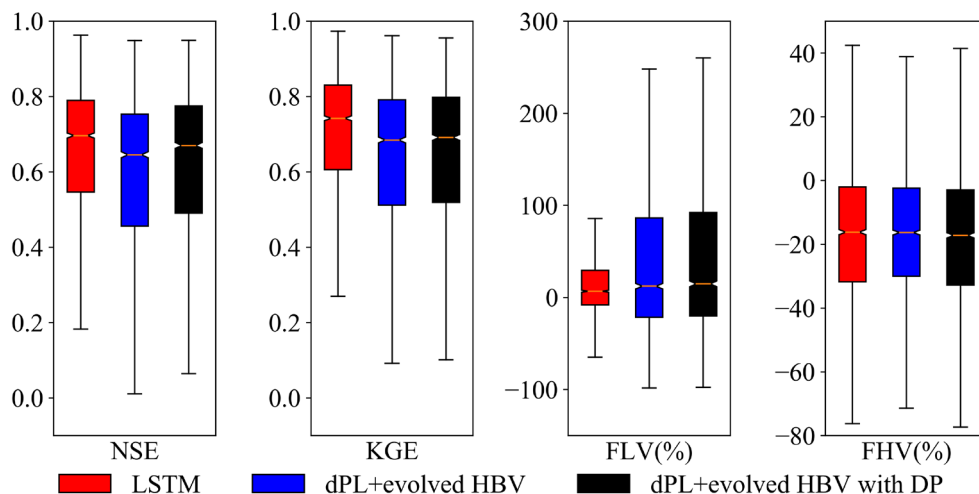
242

243 The LSTM exhibited advantages for the low flow predictions compared with the differentiable models, as shown by the FLV
244 metric (Figure 3). However, for the peak flow predictions, the LSTM and differentiable models were quite similar, and they
245 all underestimated the observed peaks (FHV in Figure 3). The underestimation for peak flows is consistent with what was
246 found in previous studies. For example, all the physical and deep learning models have significant negative peak flow bias
247 when benchmarked in the CONUS dataset (Feng et al., 2020; Kratzert et al., 2019b). We hypothesize that the systematic
248 underestimation of peaks may be partially related to bias in precipitation forcings. MSWEP is based on the ERA5 reanalysis,
249 which is known to underestimate precipitation peaks (Beck et al., 2019). Furthermore, the use of basin-averaged, daily-
250 averaged precipitation may further suppress the peaks (Chen et al., 2017). In addition, the errors with peak flow could also be
251 partly due to some numerical and structural issues with the differentiable models, e.g., numerical errors introduced by the
252 explicit and sequential solution scheme of HBV with excessive use of threshold functions that lead to different results when
253 the sequence changes, and structure limitations, e.g., deeper groundwater storage cannot feed back to the upper layers. Given
254 the commonality of this issue, we call for community efforts and collaboration to address this issue.

255

256 Both the LSTM model and the differentiable models performed well over diverse landscapes, including North America
257 (especially along the Rocky and Appalachian mountain ranges and the Southeastern Coastal Plains), Western Europe, Asia
258 (mostly Japan), the southern part of Brazil, and the northeast coast of Australia (Figure 4a and b). There are other regions
259 where none of the three models performed well, such as the longitudinally-central part of North America (Great Plains and
260 Interior Lowlands), the southern edge of Chile (with many glaciers), the Tasmania state of Australia, and the few basins in
261 Africa. These regions, for example, the Northern Great Plains and the state of Texas in the CONUS, have always been difficult
262 for all kinds of models, likely due to incorrect basin boundary, highly localized precipitation, the dry conditions with small

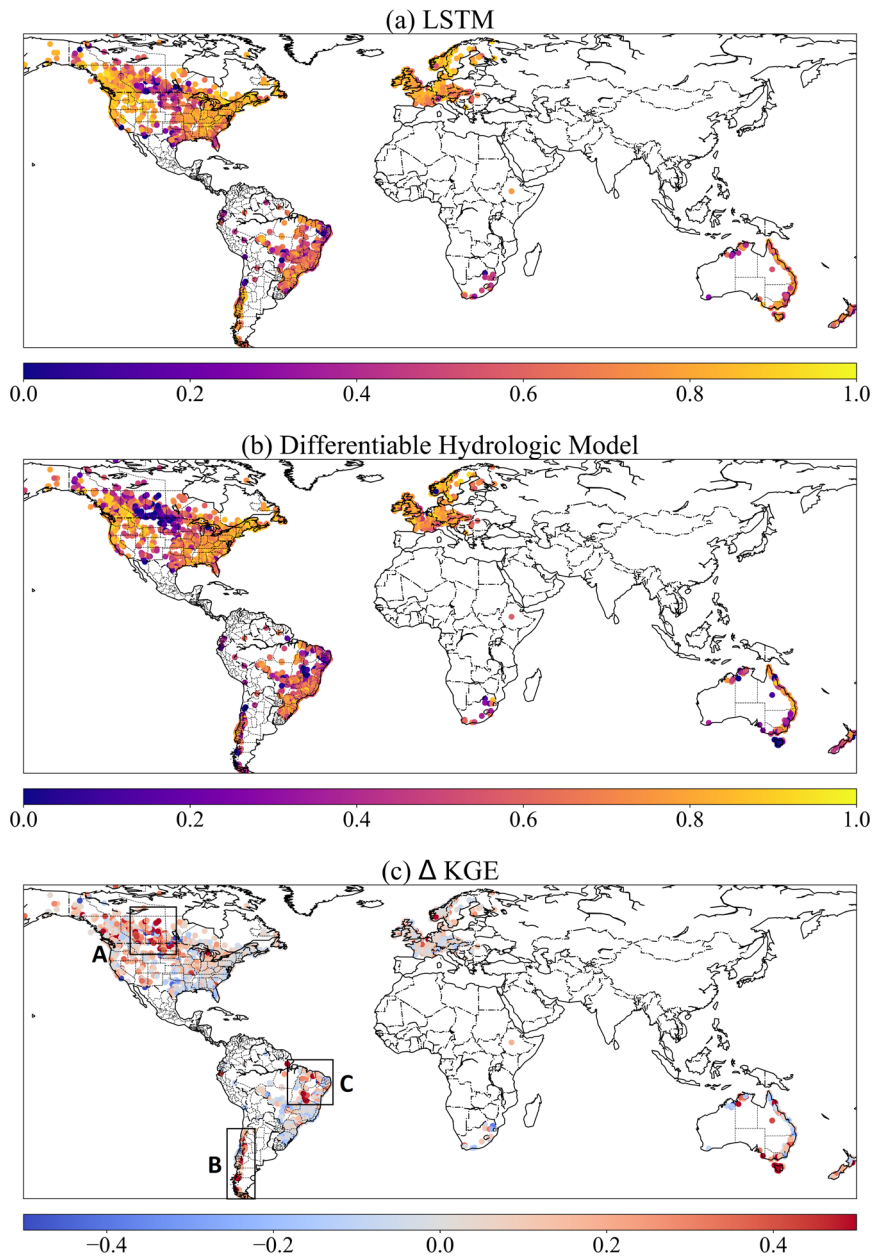
263 runoff amounts and flash flooding mechanisms (Berghuijs et al., 2014; Driscoll et al., 2002; Feng et al., 2020; Martinez and
 264 Gupta, 2010; Newman et al., 2017), to be explored below. Despite some challenges, however, these values represent currently
 265 the best metrics reported at the global scale compared to earlier studies, e.g., (Alfieri et al., 2020; Beck et al., 2017a, 2020b;
 266 Hou et al., 2023), attesting to these models' great potential as global modeling tools.
 267



268

269 *Figure 3. Performance comparison between the LSTM and differentiable models on global basins. dPL refers to the differentiable*
 270 *parameter learning framework, while “evolved HBV” refers to some modifications to improve the standard HBV model, and “with DP”*
 271 *indicates that some parameters were allowed to be dynamic rather than static. Here, the horizontal line inside the colored box represents*
 272 *the median, while the top and bottom of the colored box indicate the first and third quartiles. The bars extending from the colored boxes*
 273 *indicate 1.5 times the interquartile range from the first and third quartiles. NSE is Nash-Sutcliffe Efficiency, KGE is Kling-Gupta*
 274 *Efficiency, FLV indicates the model’s percent bias on the bottom 30% low flow range of streamflow, and FHV indicates percent bias on*
 275 *the top 2% peak flow range of streamflow.*

276



277

278 *Figure 4. The spatial patterns of different model performance and their differences shown by KGE metric. (a) the LSTM model; (b) the*
 279 *differentiable model with dynamic parameters (dPL + evolved HBV with DP); and (c) the KGE difference between two models (KGE of*
 280 *LSTM – KGE of dPL + evolved HBV with DP). Plotted in Python using Matplotlib Basemap Toolkit.*

281 3.2 Model behaviors and limitations across climate groups and regions

282 All three models' performances vary significantly across different climate groups of the global basins (Figure 5), revealing
283 their strengths and limitations. The LSTM model behaved the best in the polar, cold, and temperate groups, while the
284 performance deteriorated in the tropical and arid basins. Similar to LSTM, differentiable models showed strong performance
285 in temperate and cold groups and worse performance in tropical ones, with the worst performance in arid basins. These clusters
286 of challenging basins can also be identified on the map (Figure 4a and b). The differentiable model with dynamic parameters
287 performed better than the model with static parameters in all climate groups except the most challenging arid group. Dynamic
288 parameterization with more structural flexibility generally provides stronger modeling ability, while also showing a higher risk
289 of overfitting and degraded generalizability in basins which are very difficult to simulate. As we examine how LSTM and
290 differentiable models behave differently, we find that such differences can be attributed to processes missing from the simple
291 backbone process-based model (HBV here) as explained below. Here we use LSTM as an indicator of upper bound, that is, it
292 shows the ideal performance of a model, given the available information from forcing and input data. Thus the distance from
293 LSTM indicates either systematic and predictable forcing errors (which can be remediated by LSTM) or structural issues with
294 the differentiable model.

295

296 For example, the polar group stands out as a climate type favoring LSTM, while the cold group shows a similar but less
297 pronounced contrast, both of which may be related to HBV's physical deficiencies and forcing issues with snow undercatch.
298 For the polar (cold) groups, LSTM surprisingly had a median KGE of 0.81 (0.78) while the differentiable model only reached
299 0.62 (0.71). The polar regions include, for example, Southern Chile (in region B in Figure 4c). As glaciers can store water for
300 extended periods of time and are driven mostly by temperature rather than rainfall, it is possible for LSTM to capture the
301 temperature-driven dynamics (Lees et al., 2022) while the original HBV itself does not have a glacial module. HBV does not
302 have the ability to simulate frozen soil, sublimation or snow cover fractions. Furthermore, as snow gauges in high altitude are
303 known to suffer systematic bias due to undercatch problems (Beck et al., 2020a), LSTM can learn to address such systematic
304 bias while physical differentiable models cannot due to mass balance. For the cold regions, e.g., high-latitude regions of the
305 North American Great Plains (Region A in Figure 4c --- this also includes the Prairie Pothole Region, or PPR), HBV may
306 suffer from not having descriptions for frozen ground conditions (soil ice) which can influence infiltration, and rainfall
307 underestimation due to undercatch, ice blockage, and other potential reasons (Beck et al., 2020a). In addition, another reason
308 why LSTM and differentiable HBV may have trouble with PPR (but HBV performed especially poorly) is the countless
309 wetlands that store water until full and become connected after snowmelt and large rainfall. HBV does not have modules that
310 can describe such large-scale fill-connect-spill processes (Shaw et al., 2013; Vanderhoof et al., 2017).

311

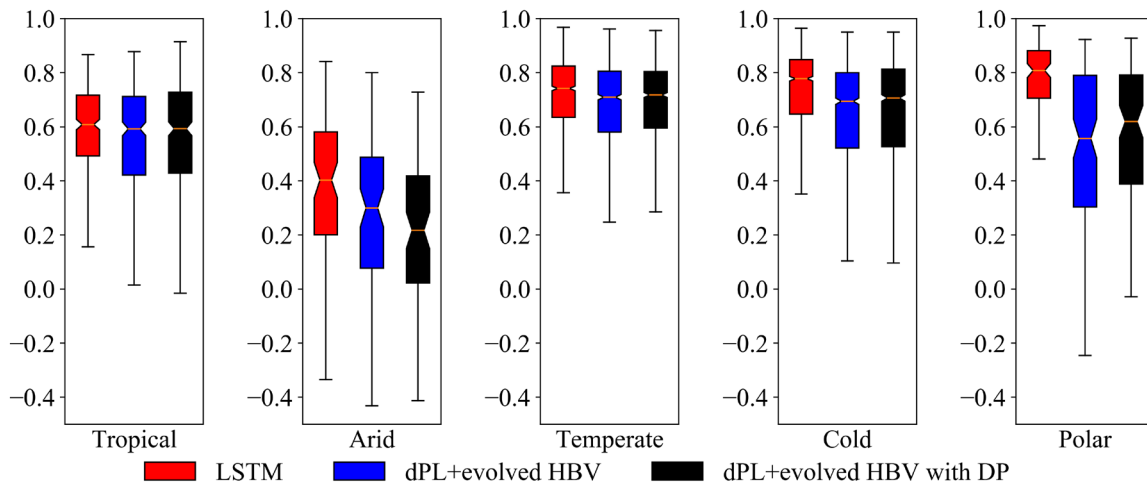
312 A more prominent challenge is the arid regions (middle CONUS, north Chile and east Brazil in Figure 1 and Figure 4). This
313 challenge can be attributed to the long duration of low flows which requires long-term memory, and flash floods which result

314 from intense short-duration storms not well represented at the daily scale. Even the LSTM model cannot retain year-long
 315 memory and cannot perform well for the baseflow (Feng et al., 2020). Because HBV has a linear reservoir for its slow-flow
 316 (lowest) bucket, it cannot generate zero base flows. Neither can it well simulate the impact of intense hourly-scale rainfall.
 317 These process improvements need to be considered in the future. Another reason for the challenge in arid regions is the lack
 318 of reservoir management modules. Arid regions tend to have water management infrastructure that significantly influences
 319 streamflow (Veldkamp et al., 2018). Since the HBV model doesn't have any module representing human impacts on the natural
 320 water cycle, the poor performance in middle Brazil in region C may have come from the missing representation of human
 321 interferences. There are large population and intensive agricultural activities in this region which could induce significant
 322 impacts on the hydrologic process. Parameter compensations apparently cannot make up for all the missing mechanisms.

323

324 The sensitivity of model performance to missing processes in the differentiable models is both good and bad news. It's good
 325 news because this means we can identify suitable or insufficient process representations by learning from data. On the other
 326 hand, this means more challenges as we need to increase the process complexity of this model before it can perform well for
 327 these basins, unlike the purely data-driven LSTM which is not explicitly concerned with physical processes.

328



329

330 *Figure 5. The performance comparison (KGE, Kling-Gupta Efficiency) of different models for five climate groups. dPL refers to the*
 331 *overall differentiable parameter learning framework, while “evolved HBV” refers to some modifications to improve the standard HBV*
 332 *model, and “with DP” indicates that some parameters were allowed to be dynamic rather than static. Here, the horizontal line inside the*
 333 *colored box represents the median, while the top and bottom of the colored box indicate the first and third quartiles. The bars extending*
 334 *from the colored boxes indicate 1.5 times the interquartile range from the first and third quartiles.*

335 3.3 Spatial generalization for prediction in ungauged regions

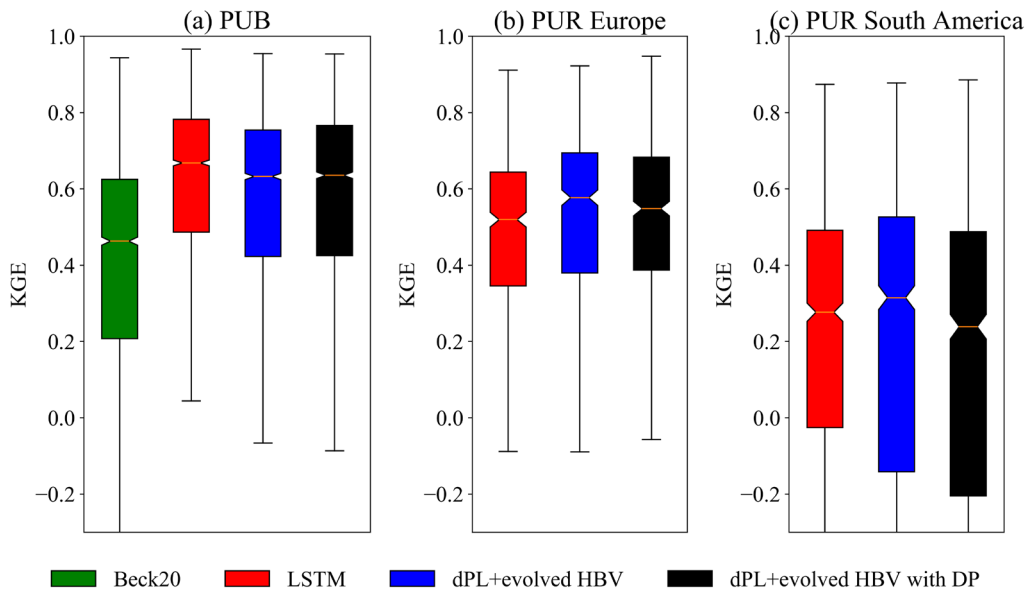
336 While LSTM maintains mild advantages over differentiable models in data-dense settings, it was outperformed by
 337 differentiable models in a highly data-scarce scenario. As mentioned above, the data-dense setting was tested in the randomized

338 holdout test called prediction in ungauged basins (PUB), while the data-scarce scenario was tested in the regional holdout test,
339 or prediction in ungauged regions (PUR). In the global PUB test, LSTM has a small edge (median KGE=0.67) over
340 differentiable models (median KGE=0.64). Both were noticeably higher than the traditional regionalization method using
341 linear transfer functions reported by Beck et al. (2020b) (Beck20, median KGE=0.46), which already represents the previous
342 state-of-the-art performance of global parameter regionalization. Differentiable modeling does not rely on strong assumptions
343 of the functional form for the parameter transfer function. It leverages the powerful ability of neural networks to represent
344 complicated functions, and automatically learns robust and generalizable relationships between geographic attributes and
345 physical model parameters from large data. Therefore, we can expect significant performance advantages from differentiable
346 modeling compared to traditional methods relying on linear transfer functions. In the PUR scenario where European basins
347 were held out for testing, differentiable models (median KGE=0.58) performed significantly better (p-value less than 0.01
348 using the one-sided Wilcoxon signed-rank test) than LSTM (median KGE=0.52). In the South American PUR experiment,
349 lower performance was seen for all models which can be expected considering the prediction difficulties in this region even
350 for the in-sample scenario (Region B and C in Figure 4). The median KGE of LSTM is 0.28 while the differentiable model
351 with static parameters achieves a higher median KGE of 0.31 for the PUR scenario. It seemed that the differentiable model
352 with dynamic parameterization was somewhat overfitted in this case, resulting in a median KGE that was lower than the static-
353 parameter differentiable model. We do not have PUR results from traditional models available to compare against, since this
354 is a very challenging issue for traditional regionalization methods to make predictions across continents.

355

356 With these results, we show that differentiable models have demonstrated a high simulation capability that cannot be obtained
357 with traditional parameter regionalization approaches, and also provide a robust extrapolation capability in large data-sparse
358 regions that is stronger than purely data-driven models like LSTM. This conclusion was not only verified in the USA, but now
359 has also been confirmed in global catchments with generalization tests including prediction in neighboring ungauged basins
360 and cross-continent predictions, each of which have different conditions with respect to data availability and density.

361



362

363 *Figure 6. The performance comparison (KGE, Kling-Gupta Efficiency) of different models for spatial generalization tests. (a) Random*
 364 *hold-out test for prediction in ungauged basins (PUB), (b) and (c) holding out all the basins in Europe or South America, respectively,*
 365 *for cross-continent predictions in ungauged regions (PUR). Beck20 refers to a traditional regionalization method using linear transfer*
 366 *functions (Beck et al., 2020b), LSTM is the purely data-driven long short-term memory network, dPL refers to the differentiable*
 367 *parameter learning framework, while “evolved HBV” refers to some modifications to improve the standard HBV model, and “with DP”*
 368 *indicates that some parameters were allowed to be dynamic rather than static. Here, the horizontal line inside the colored box represents*
 369 *the median, while the top and bottom of the colored box indicate the first and third quartiles. The bars extending from the colored boxes*
 370 *indicate 1.5 times the interquartile range from the first and third quartiles.*

371 3.4 Predicting untrained variables

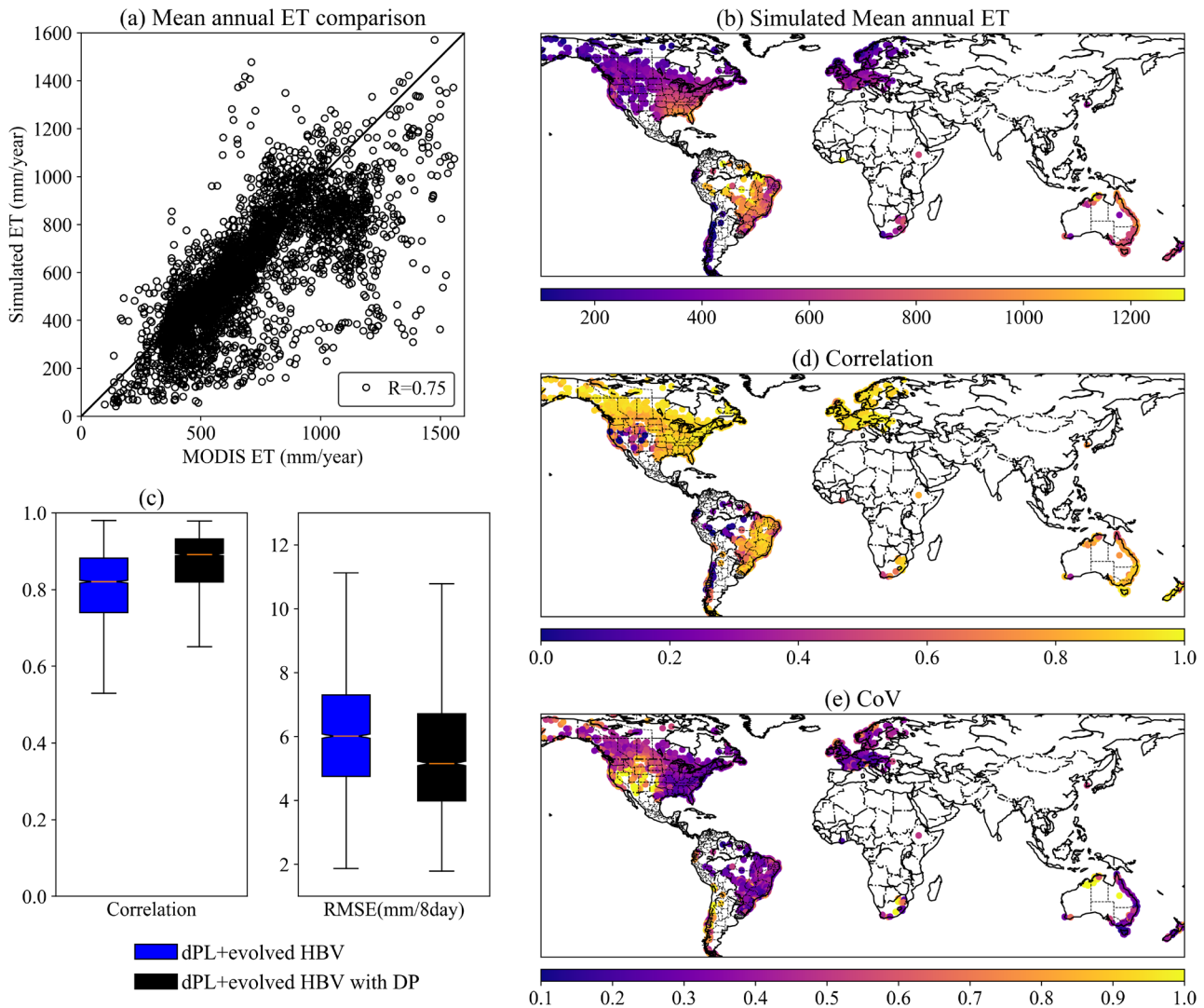
372 The evapotranspiration (ET) simulations from differentiable models are consistent with independent MODIS satellite estimates
 373 of ET in both temporal dynamics and spatial patterns. We did not use any ET observations as training targets to supervise the
 374 differentiable models. At the global scale, the mean annual ET comparison shows overall consistency with MODIS, with most
 375 basins lying close to the 1:1 line and a correlation of 0.75 for all the basins (Figure 7a). Spatially, the model was able to
 376 represent energy limitations in the cold regions, e.g., high-latitude North America and Europe, and water limitations, e.g.,
 377 southwestern US and arid basins of Australia (Figure 7a and b). The model also represented high ET in basins adjacent to the
 378 Amazon forest, those along the US southeastern and Australian coast. Temporally, the median correlation of ET time series
 379 between simulations and MODIS products achieves 0.82 and 0.89 for two differentiable models in 3753 basins, respectively
 380 (Figure 7c).

381

382 The ET simulations show high correlation with MODIS in most North American and European basins (Figure 7d), in line with
 383 the good performance of streamflow modeling in these regions. However, the correlation is relatively lower in South America
 384 but the coefficient of variation of ET residuals (CoV, the ratio of standard deviation of ET residuals to the annual mean) is also

385 small (Figure 7e), in part because the ET here is large and less driven by the seasonal energy cycle (Niu et al., 2017). MODIS
386 ET itself is not the ground truth and always has large uncertainties in Amazonia regions due to the cloud coverage and
387 difficulties for observation (Hilker et al., 2015; Xu et al., 2019). Furthermore, the simulations could be negatively influenced
388 by the data quality issues with streamflow records in these regions. Upon examining the records, some stations in South
389 America show unrealistic hydrographs that may indicate data processing errors. To address such issues in the future, more in-
390 depth data screening and correction or constraining the model using datasets other than streamflow, e.g., eddy covariance flux
391 data, should be considered. The CoV is less than 0.3 for most of the world, showing that ET errors are mostly small relative to
392 its annual averages (Figure 7e). Noticeable exceptions are US southwest, where ET varies strongly from year to year and is
393 highly dependent on the precipitation, and Chile, where glaciers and deserts are both present, posing challenges to the model.
394 As the present study is basin-focused, we will leave the evaluation of global gridded ET to future work.

395



396

397 *Figure 7. The comparison between simulated ET from the differentiable hydrologic models and independent MODIS ET product. (a)*
 398 *mean annual ET comparison, (b) simulated mean annual ET for global basins, (c) boxplots for the temporal dynamic evaluation by*
 399 *correlation and RMSE, (d) correlation and (e) coefficient of variation for ET comparison in global basins. Maps plotted in Python using*
 400 *Matplotlib Basemap Toolkit.*

401 3.5 Further discussion

402 Compared to the LSTM model which only outputs discharge simulations, differentiable models offer a suite of interpretable
 403 variables including ET, soil water, recharge, baseflow, etc., thus providing a comprehensive description for the hydrologic
 404 cycle and far better interpretability. To create a new differentiable model or turn an existing model into a differentiable one,
 405 we need to implement the model on a differentiable platform like PyTorch, Tensorflow, or JAX, while better enabling model
 406 parallelism in order to maximally leverage the computing power of modern graphical processing units (GPUs). If a model

407 contains mostly explicit calculations, automatic differentiation (AD) offered by the above platforms can effortlessly provide
408 gradient calculations, requiring only a syntax-level translation which can nowadays be done easily. Sometimes, a limited
409 amount of adjustments are needed to turn non-differentiable operations into equivalent differentiable ones. However, when a
410 model contains iterative solutions to nonlinear systems, large matrix solvers or constrained optimizations, we can employ the
411 adjoint method (Song et al., 2023). The adjoint method explicitly defines the gradient-calculation method and alters the order
412 of calculations so iteration is avoided during gradient calculations, which can dramatically reduce memory demand and
413 improve efficiency. Another important consideration is the effective use of parallelism and the modern computing
414 infrastructure for AI (i.e., GPUs). In our context, the regionalized parameterization (in this case, training one neural network
415 on a large amount of basins), which is crucial to ensuring the generalizability of the model, requires going through large data
416 in high-throughput parallelism. Embracing parallelism may necessitate some coding adjustments. At this point, several
417 versions of differentiable hydrologic models have been proposed with varying complexities and different handling of
418 parameterization, post-processing (which we didn't use in this study, as it can interfere with interpretability of the internal
419 variables, mass balances, and the sensitivity to inputs encoded by the process-based components), and dynamical parameters.
420 Across geoscientific domains, differentiable ecosystem (Aboelyazeed et al., 2023; Zhao et al., 2019), flow and routing (Bindas
421 et al., 2024), water quality (Rahmani et al., 2023), and ice sheet (Bolibar et al., 2023) models have already been demonstrated.
422

423 The challenges facing the differentiable models in this study include not only missing processes like reservoir management,
424 ground ice, and glaciers, but also large errors in meteorological forcings and streamflow target data. Substantial bias could
425 exist in precipitation, e.g., due to snow-gauge undercatch (Hou et al., 2023), or in discharge, e.g., streamflow are measured
426 using different approaches which exhibit large variability; for another example, gridded climate forcing data often consistently
427 underestimate the magnitudes of heavy storms (Beck et al., 2017b). While LSTM can easily adapt to systematic bias, such
428 forcing errors put the differentiable models under stress because they cannot reconcile streamflow observations with such
429 forcings given the constraint of mass balances. If our objective is to learn core physics and parameterizations that are reliable
430 despite forcing discrepancies, we can set up forcing data correction layers that can, to some extent, shield the core processes
431 from being influenced by such errors. This will be an important aspect of future work to ensure reliable prediction of future
432 water resources.

433
434 The backbone of a differentiable process-based model thus serves as a double-edged sword: when such backbones are
435 essentially correct, they serve as a stabilizing element of the model that mitigates overfitting and improves generalization;
436 when they lack critical processes or when observations have large, unexplained bias, they can drag down model performance
437 and cause compensation between processes. However, the limitations are tractable: future work can gradually incorporate
438 critical processes and include more observations to constrain the learning process, making sure each addition is valuable and
439 accretive. The research community collectively has already substantial experience in evolving earth system models to include
440 many processes. We expect some processes to be invited back in the differentiable modeling framework. Nevertheless, with

441 differentiable modeling, we now have a new tool that was not previously available: highly flexible deep neural networks that
442 can be placed anywhere in the model, which provide a systematic way of managing model complexity. With their help, such
443 model evolution may take much less time than previously required. However, we still expect the development cycle to take
444 longer than for purely data-driven models like LSTM, requiring us to view differentiable models as evolving rather than static
445 entities, which need a bit of patience while maturing.

446

447 This study builds a benchmark and a basis for model selection and diagnosis for the next-generation global hydrologic
448 modeling, which previously did not learn from such large observations. With rigorous tests at the global scale, this study proves
449 that differentiable models are strong candidates as global water models. With powerful spatial generalization ability, they can
450 be applied to characterizing the hydrologic processes in ungauged regions by leveraging learned information in data-rich
451 continents. Differentiable models in this study have already learned the generalizable and robust relationships between
452 geographic attributes and physical model parameters from thousands of global catchments. Therefore, these models can be
453 easily applied towards providing seamless global hydrologic modeling with parameters directly generated from worldwide
454 geographic attributes. Future work can use such models to produce global hydrologic fluxes while enhancing some process
455 representations in extremely arid, glaciated, or heavily human-influenced basins.

456 **4. Conclusions**

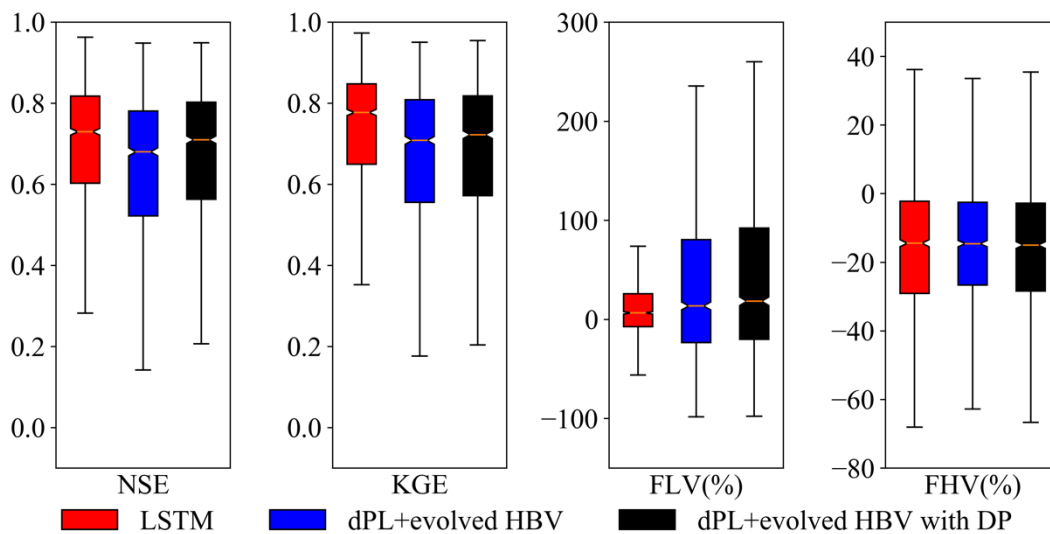
457 In this work, we used both purely data-driven models and, for the first time, physics-informed, differentiable models to simulate
458 rainfall-runoff processes in 3753 global basins. Both types of models achieved overall highly competitive performance for
459 global basins with diverse climate conditions, yielding median KGE values close to or higher than 0.7 which is state-of-the-
460 art at this large scale. The LSTM still achieved the best performance for the temporal generalization test, but the differentiable
461 HBV models with evolved structure (δ HBV-globe1.0-hydroDL) approach the LSTM's performance level. Furthermore, the
462 spatial generalization experiments highlighted the stronger regionalization and extrapolation ability of differentiable models
463 than LSTM, demonstrating its promise to be applied to data-scarce regions in the world. Routing is not included in this work
464 and will be investigated in the future, possibly also with differentiable approaches (Bindas et al., 2022).

465

466 Different models appear to have generally consistent spatial performance patterns, though obvious distinctions stand out in
467 several local regions. All models achieve good performance in the temperate and cold climate groups, while they all behave
468 unsatisfactorily in the arid group. For the polar group, the differentiable model performed significantly worse than the LSTM.
469 Without any physical constraints, LSTM shows strong power in simulating storage (snow and glacier) dominated processes,
470 while differentiable models are limited by the structure of their physical backbone model, which in this case does not simulate
471 multiyear ice buildup and melt. Another limitation could be soil sealing processes in extremely arid regions. These regional
472 performance comparisons thus reveal some deficiencies of the physical backbone in δ HBV that cannot be mitigated even by

473 advanced neural network-based parameterization. These insights provide directions for future improvements. Different from
 474 purely data-driven models only trained by the target variable, differentiable models constrained by the physical backbone can
 475 give accurate simulations for a full set of hydrologic variables in the water cycle including evapotranspiration, snow water
 476 equivalent, water storage, infiltration and baseflow. As some process limitations are addressed in the future, we believe
 477 differentiable models will be strong candidates for the next generation global water models to characterize and predict the
 478 hydrologic processes in ungauged regions across the world.

479 Appendix



480

481 **Figure A1. Performance comparison on the 1675 subset basins with long-term streamflow records (at least 15 years' worth**
 482 **of streamflow data available in the training period and 5 years' worth of data available in the testing period, not necessarily**
 483 **continuous). Other items are the same as in Figure 3.**

484

485 Author contributions

486 DF and CS conceived this study. DF set up the hydrologic models and ran all the experiments. DF and CS performed the major
 487 analysis, with HB, JdB, RKS, YS, YW and MP contributing substantially to the discussions on the methodology and results.
 488 HB provided the global dataset and the benchmark results from a traditional regionalization scheme. JL prepared the ET
 489 product for comparison. DF wrote the initial draft and CS revised the manuscript. HB, JdB, RKS, YS, YW, and KL
 490 substantially edited the manuscript.

491 **Financial support**

492 DF was supported by the National Science Foundation Award EAR-2221880. This work was also partially supported and
493 inspired by the Young Scientists Summer Program (YSSP) of International Institute for Applied Systems Analysis (IIASA).
494 JL was supported by Google.org's AI Impacts Challenge Grant 1904-57775. CS and KL were supported by Cooperative
495 Institute for Research to Operations in Hydrology (CIROH), award number A22-0307-S003. Computation was partially
496 supported by the National Science Foundation Major Research Instrumentation Award PHY-2018280.

497 **Code and Data Availability**

498 The source codes for the differentiable hydrologic models can be accessed at <https://doi.org/10.5281/zenodo.7091334>, and this
499 study evaluates these models at global scale. The MOD16A2GF ET product can be downloaded at
500 <https://lpdaac.usgs.gov/products/mod16a2gfv061/>. Meteorological forcing datasets MSWEP and MSWX can be downloaded
501 at <https://www.gloh2o.org/mswep/> and <https://www.gloh2o.org/mswx/>, respectively. The streamflow observations used in this
502 study were initially compiled by Beck, Pan, et al., (2020b) and can be accessed from the original data sources including the
503 United States Geological Survey (USGS) National Water Information System (NWIS; <https://waterdata.usgs.gov/nwis>), the
504 Global Runoff Data Centre (GRDC; <https://grdc.bafg.de>), the HidroWeb portal of the Brazilian Agência Nacional de Águas
505 (<https://www.snirh.gov.br/hidroweb>), the European Water Archive (EWA) of EURO-FRIEND-Water
506 (https://www.bafg.de/GRDC/EN/04_spcldtbss/42_EWA/ewa.html) and the CCM2-JRC CCM River and Catchment Database
507 (<https://data.jrc.ec.europa.eu/collection/ccm>), Water Survey of Canada (WSC) National Water Data Archive (HYDAT;
508 <https://wateroffice.ec.gc.ca/>), the Australian Bureau of Meteorology (BoM; <http://www.bom.gov.au/waterdata/>), and the
509 Chilean Center for Climate and Resilience Research (CR2) website (<https://www.cr2.cl/datos-de-caudales/>).

510 **References**

- 511 Aboelyzeed, D., Xu, C., Hoffman, F. M., Liu, J., Jones, A. W., Rackauckas, C., Lawson, K., and Shen, C.: A differentiable,
512 physics-informed ecosystem modeling and learning framework for large-scale inverse problems: demonstration with
513 photosynthesis simulations, *Biogeosciences*, 20, 2671–2692, <https://doi.org/10.5194/bg-20-2671-2023>, 2023.
- 514 Alfieri, L., Lorini, V., Hirpa, F. A., Harrigan, S., Zsoter, E., Prudhomme, C., and Salamon, P.: A global streamflow reanalysis
515 for 1980–2018, *Journal of Hydrology X*, 6, 100049, <https://doi.org/10.1016/j.hydroa.2019.100049>, 2020.
- 516 Beck, H. E., van Dijk, A. I. J. M., de Roo, A., Dutra, E., Fink, G., Orth, R., and Schellekens, J.: Global evaluation of runoff
517 from 10 state-of-the-art hydrological models, *Hydrology and Earth System Sciences*, 21, 2881–2903,
518 <https://doi.org/10.5194/hess-21-2881-2017>, 2017a.
- 519 Beck, H. E., Vergopolan, N., Pan, M., Levizzani, V., van Dijk, A. I. J. M., Weedon, G. P., Brocca, L., Pappenberger, F.,
520 Huffman, G. J., and Wood, E. F.: Global-scale evaluation of 22 precipitation datasets using gauge observations and

- 521 hydrological modeling, *Hydrology and Earth System Sciences*, 21, 6201–6217, <https://doi.org/10.5194/hess-21-6201-2017>,
522 2017b.
- 523 Beck, H. E., van Dijk, A. I. J. M., Levizzani, V., Schellekens, J., Miralles, D. G., Martens, B., and de Roo, A.: MSWEP: 3-
524 hourly 0.25° global gridded precipitation (1979-2015) by merging gauge, satellite, and reanalysis data, *Hydrology and Earth*
525 *System Sciences*, 21, 589–615, <https://doi.org/10.5194/hess-21-589-2017>, 2017c.
- 526 Beck, H. E., Wood, E. F., Pan, M., Fisher, C. K., Miralles, D. G., Dijk, A. I. J. M. van, McVicar, T. R., and Adler, R. F.:
527 MSWEP V2 Global 3-Hourly 0.1° Precipitation: Methodology and Quantitative Assessment, *Bulletin of the American*
528 *Meteorological Society*, 100, 473–500, <https://doi.org/10.1175/BAMS-D-17-0138.1>, 2019.
- 529 Beck, H. E., Wood, E. F., McVicar, T. R., Zambrano-Bigiarini, M., Alvarez-Garreton, C., Baez-Villanueva, O. M., Sheffield,
530 J., and Karger, D. N.: Bias correction of global high-resolution precipitation climatologies using streamflow observations from
531 9372 catchments, *Journal of Climate*, 33, 1299–1315, <https://doi.org/10.1175/JCLI-D-19-0332.1>, 2020a.
- 532 Beck, H. E., Pan, M., Lin, P., Seibert, J., Dijk, A. I. J. M. van, and Wood, E. F.: Global fully distributed parameter
533 regionalization based on observed streamflow from 4,229 headwater catchments, *Journal of Geophysical Research:*
534 *Atmospheres*, 125, e2019JD031485, <https://doi.org/10.1029/2019JD031485>, 2020b.
- 535 Beck, H. E., van Dijk, A. I. J. M., Larraondo, P. R., McVicar, T. R., Pan, M., Dutra, E., and Miralles, D. G.: MSWX: Global
536 3-hourly 0.1° bias-corrected meteorological data including near real-time updates and forecast ensembles, *Bulletin of the*
537 *American Meteorological Society*, 103, E710–E732, <https://doi.org/10.1175/BAMS-D-21-0145.1>, 2022.
- 538 Berghuijs, W. R., Sivapalan, M., Woods, R. A., and Savenije, H. H. G.: Patterns of similarity of seasonal water balances: A
539 window into streamflow variability over a range of time scales, *Water Resources Research*, 50, 5638–5661,
540 <https://doi.org/10.1002/2014WR015692>, 2014.
- 541 Bergström, S.: Development and application of a conceptual runoff model for Scandinavian catchments, PhD Thesis, Swedish
542 Meteorological and Hydrological Institute (SMHI), Norköping, Sweden, 1976.
- 543 Bergström, S.: The HBV model - its structure and applications, Swedish Meteorological and Hydrological Institute (SMHI),
544 Norrköping, Sweden, 1992.
- 545 Bindas, T., Tsai, W.-P., Liu, J., Rahmani, F., Feng, D., Bian, Y., Lawson, K., and Shen, C.: Improving river routing using a
546 differentiable Muskingum-Cunge model and physics-informed machine learning, *Water Resources Research*, 60,
547 e2023WR035337, <https://doi.org/10.1029/2023WR035337>, 2024.
- 548 Bolibar, J., Sapienza, F., Maussion, F., Lguensat, R., Wouters, B., and Pérez, F.: Universal differential equations for glacier
549 ice flow modelling, *Geoscientific Model Development*, 16, 6671–6687, <https://doi.org/10.5194/gmd-16-6671-2023>, 2023.
- 550 Burek, P., Satoh, Y., Kahil, T., Tang, T., Greve, P., Smilovic, M., Guillaumot, L., Zhao, F., and Wada, Y.: Development of
551 the Community Water Model (CWatM v1.04) – a high-resolution hydrological model for global and regional assessment of
552 integrated water resources management, *Geoscientific Model Development*, 13, 3267–3298, [https://doi.org/10.5194/gmd-13-](https://doi.org/10.5194/gmd-13-3267-2020)
553 [3267-2020](https://doi.org/10.5194/gmd-13-3267-2020), 2020.
- 554 Chaemchuen, P., Song, Y., Rahmani, F., Zhi, W., Li, L., Liu, X., Boyer, E., Bindas, T., Lawson, K., and Shen, C.: Deep
555 learning insights into suspended sediment concentrations across the conterminous United States: Strengths and limitations,
556 <https://papers.ssrn.com/abstract=4322321>, 11 January 2023.

- 557 Chen, B., Krajewski, W. F., Liu, F., Fang, W., and Xu, Z.: Estimating instantaneous peak flow from mean daily flow,
558 Hydrology Research, 48, 1474–1488, <https://doi.org/10.2166/nh.2017.200>, 2017.
- 559 Cui, G., Anderson, M., and Bales, R.: Mapping of snow water equivalent by a deep-learning model assimilating snow
560 observations, J. Hydrol., 616, 128835, <https://doi.org/10.1016/j.jhydrol.2022.128835>, 2023.
- 561 Driscoll, D. G., Carter, J. M., Williamson, J. E., and Putnam, L. D.: Hydrology of the Black Hills Area, South Dakota, 2002.
- 562 Fang, K. and Shen, C.: Near-real-time forecast of satellite-based soil moisture using long short-term memory with an adaptive
563 data integration kernel, J. Hydrometeor., 21, 399–413, <https://doi.org/10.1175/jhm-d-19-0169.1>, 2020.
- 564 Fang, K., Shen, C., Kifer, D., and Yang, X.: Prolongation of SMAP to spatiotemporally seamless coverage of continental U.S.
565 using a deep learning neural network, Geophys. Res. Lett., 44, 11,030–11,039, <https://doi.org/10.1002/2017gl075619>, 2017.
- 566 Fang, K., Pan, M., and Shen, C.: The value of SMAP for long-term soil moisture estimation with the help of deep learning,
567 IEEE Trans. Geosci. Remote Sensing, 57, 2221–2233, <https://doi.org/10.1109/TGRS.2018.2872131>, 2019.
- 568 Fang, K., Kifer, D., Lawson, K., Feng, D., and Shen, C.: The data synergy effects of time-series deep learning models in
569 hydrology, Water Resources Research, 58, e2021WR029583, <https://doi.org/10.1029/2021WR029583>, 2022.
- 570 Feng, D., Fang, K., and Shen, C.: Enhancing streamflow forecast and extracting insights using long-short term memory
571 networks with data integration at continental scales, Water Resources Research, 56, e2019WR026793,
572 <https://doi.org/10.1029/2019WR026793>, 2020.
- 573 Feng, D., Lawson, K., and Shen, C.: Mitigating prediction error of deep learning streamflow models in large data-sparse
574 regions with ensemble modeling and soft data, Geophysical Research Letters, 48, e2021GL092999,
575 <https://doi.org/10.1029/2021GL092999>, 2021.
- 576 Feng, D., Liu, J., Lawson, K., and Shen, C.: Differentiable, learnable, regionalized process-based models with multiphysical
577 outputs can approach state-of-the-art hydrologic prediction accuracy, Water Resources Research, 58, e2022WR032404,
578 <https://doi.org/10.1029/2022WR032404>, 2022.
- 579 Feng, D., Beck, H., Lawson, K., and Shen, C.: The suitability of differentiable, physics-informed machine learning hydrologic
580 models for ungauged regions and climate change impact assessment, Hydrology and Earth System Sciences, 27, 2357–2373,
581 <https://doi.org/10.5194/hess-27-2357-2023>, 2023.
- 582 Gupta, H. V., Kling, H., Yilmaz, K. K., and Martinez, G. F.: Decomposition of the mean squared error and NSE performance
583 criteria: Implications for improving hydrological modelling, Journal of Hydrology, 377, 80–91,
584 <https://doi.org/10.1016/j.jhydrol.2009.08.003>, 2009.
- 585 Hagemann, S., Chen, C., Clark, D. B., Folwell, S., Gosling, S. N., Haddeland, I., Hanasaki, N., Heinke, J., Ludwig, F., Voss,
586 F., and Wiltshire, A. J.: Climate change impact on available water resources obtained using multiple global climate and
587 hydrology models, Earth System Dynamics, 4, 129–144, <https://doi.org/10.5194/esd-4-129-2013>, 2013.
- 588 Hansen, L. D., Stokholm-Bjerregaard, M., and Durdevic, P.: Modeling phosphorous dynamics in a wastewater treatment
589 process using Bayesian optimized LSTM, Computers & Chemical Engineering, 160, 107738,
590 <https://doi.org/10.1016/j.compchemeng.2022.107738>, 2022.
- 591 Hargreaves, G. H.: Defining and using reference evapotranspiration, Journal of Irrigation and Drainage Engineering, 120,
592 1132–1139, [https://doi.org/10.1061/\(ASCE\)0733-9437\(1994\)120:6\(1132\)](https://doi.org/10.1061/(ASCE)0733-9437(1994)120:6(1132)), 1994.

- 593 Hattermann, F. F., Krysanova, V., Gosling, S. N., Dankers, R., Daggupati, P., Donnelly, C., Flörke, M., Huang, S., Motovilov,
594 Y., Buda, S., Yang, T., Müller, C., Leng, G., Tang, Q., Portmann, F. T., Hagemann, S., Gerten, D., Wada, Y., Masaki, Y.,
595 Alemayehu, T., Satoh, Y., and Samaniego, L.: Cross-scale intercomparison of climate change impacts simulated by regional
596 and global hydrological models in eleven large river basins, *Climatic Change*, 141, 561–576, <https://doi.org/10.1007/s10584->
597 016-1829-4, 2017.
- 598 Hilker, T., Lyapustin, A. I., Hall, F. G., Myneni, R., Knyazikhin, Y., Wang, Y., Tucker, C. J., and Sellers, P. J.: On the
599 measurability of change in Amazon vegetation from MODIS, *Remote Sensing of Environment*, 166, 233–242,
600 <https://doi.org/10.1016/j.rse.2015.05.020>, 2015.
- 601 Hochreiter, S. and Schmidhuber, J.: Long Short-Term Memory, *Neural Computation*, 9, 1735–1780,
602 <https://doi.org/10.1162/neco.1997.9.8.1735>, 1997.
- 603 Höge, M., Scheidegger, A., Baity-Jesi, M., Albert, C., and Fenicia, F.: Improving hydrologic models for predictions and
604 process understanding using neural ODEs, *Hydrology and Earth System Sciences*, 26, 5085–5102,
605 <https://doi.org/10.5194/hess-26-5085-2022>, 2022.
- 606 Hou, Y., Guo, H., Yang, Y., and Liu, W.: Global Evaluation of Runoff Simulation From Climate, *Hydrological and Land*
607 *Surface Models*, *Water Resources Research*, 59, e2021WR031817, <https://doi.org/10.1029/2021WR031817>, 2023.
- 608 Jayakrishnan, R., Srinivasan, R., Santhi, C., and Arnold, J. G.: Advances in the application of the SWAT model for water
609 resources management, *Hydrological Processes*, 19, 749–762, <https://doi.org/10.1002/hyp.5624>, 2005.
- 610 Jiang, S., Zheng, Y., and Solomatine, D.: Improving AI system awareness of geoscience knowledge: Symbiotic integration of
611 physical approaches and deep learning, *Geophysical Research Letters*, 47, e2020GL088229,
612 <https://doi.org/10.1029/2020GL088229>, 2020.
- 613 Kling, H., Fuchs, M., and Paulin, M.: Runoff conditions in the upper Danube basin under an ensemble of climate change
614 scenarios, *Journal of Hydrology*, 424–425, 264–277, <https://doi.org/10.1016/j.jhydrol.2012.01.011>, 2012.
- 615 Konapala, G., Kao, S.-C., Painter, S. L., and Lu, D.: Machine learning assisted hybrid models can improve streamflow
616 simulation in diverse catchments across the conterminous US, *Environ. Res. Lett.*, 15, 104022, <https://doi.org/10.1088/1748->
617 9326/aba927, 2020.
- 618 Kraft, B., Jung, M., Körner, M., Koirala, S., and Reichstein, M.: Towards hybrid modeling of the global hydrological cycle,
619 *Hydrology and Earth System Sciences*, 26, 1579–1614, <https://doi.org/10.5194/hess-26-1579-2022>, 2022.
- 620 Kratzert, F., Klotz, D., Herrnegger, M., Sampson, A. K., Hochreiter, S., and Nearing, G. S.: Toward improved predictions in
621 ungauged basins: Exploiting the power of machine learning, *Water Resources Research*, 55, 11344–11354,
622 <https://doi.org/10/gg4ck8>, 2019a.
- 623 Kratzert, F., Klotz, D., Shalev, G., Klambauer, G., Hochreiter, S., and Nearing, G.: Towards learning universal, regional, and
624 local hydrological behaviors via machine learning applied to large-sample datasets, *Hydrology and Earth System Sciences*,
625 23, 5089–5110, <https://doi.org/10.5194/hess-23-5089-2019>, 2019b.
- 626 Lees, T., Buechel, M., Anderson, B., Slater, L., Reece, S., Coxon, G., and Dadson, S. J.: Benchmarking data-driven rainfall–
627 runoff models in Great Britain: a comparison of long short-term memory (LSTM)-based models with four lumped conceptual
628 models, *Hydrology and Earth System Sciences*, 25, 5517–5534, <https://doi.org/10.5194/hess-25-5517-2021>, 2021.

- 629 Lees, T., Reece, S., Kratzert, F., Klotz, D., Gauch, M., De Bruijn, J., Kumar Sahu, R., Greve, P., Slater, L., and Dadson, S. J.:
630 Hydrological concept formation inside long short-term memory (LSTM) networks, *Hydrology and Earth System Sciences*, 26,
631 3079–3101, <https://doi.org/10.5194/hess-26-3079-2022>, 2022.
- 632 Liu, J., Bian, Y., Lawson, K., and Shen, C.: Probing the limit of hydrologic predictability with the Transformer network, *J.*
633 *Hydrol.*, 637, 131389, <https://doi.org/10.1016/j.jhydrol.2024.131389>, 2024.
- 634 Mai, J., Shen, H., Tolson, B. A., Gaborit, É., Arsenault, R., Craig, J. R., Fortin, V., Fry, L. M., Gauch, M., Klotz, D., Kratzert,
635 F., O’Brien, N., Princz, D. G., Rasiya Koya, S., Roy, T., Seglenieks, F., Shrestha, N. K., Temgoua, A. G. T., Vionnet, V., and
636 Waddell, J. W.: The Great Lakes Runoff Intercomparison Project Phase 4: the Great Lakes (GRIP-GL), *Hydrology and Earth*
637 *System Sciences*, 26, 3537–3572, <https://doi.org/10.5194/hess-26-3537-2022>, 2022.
- 638 Maidment, D. R.: Conceptual Framework for the National Flood Interoperability Experiment, *JAWRA Journal of the*
639 *American Water Resources Association*, 53, 245–257, <https://doi.org/10/f97pz3>, 2017.
- 640 Martinez, G. F. and Gupta, H. V.: Toward improved identification of hydrological models: A diagnostic evaluation of the
641 “abcd” monthly water balance model for the conterminous United States, *Water Resources Research*, 46,
642 <https://doi.org/10.1029/2009WR008294>, 2010.
- 643 Mizukami, N., Clark, M. P., Newman, A. J., Wood, A. W., Gutmann, E. D., Nijssen, B., Rakovec, O., and Samaniego, L.:
644 Towards seamless large-domain parameter estimation for hydrologic models, *Water Resources Research*, 53, 8020–8040,
645 <https://doi.org/10/gcg2dm>, 2017.
- 646 Müller Schmied, H., Eisner, S., Franz, D., Wattenbach, M., Portmann, F. T., Flörke, M., and Döll, P.: Sensitivity of simulated
647 global-scale freshwater fluxes and storages to input data, hydrological model structure, human water use and calibration,
648 *Hydrology and Earth System Sciences*, 18, 3511–3538, <https://doi.org/10.5194/hess-18-3511-2014>, 2014.
- 649 Nash, J. E. and Sutcliffe, J. V.: River flow forecasting through conceptual models part I — A discussion of principles, *Journal*
650 *of Hydrology*, 10, 282–290, [https://doi.org/10.1016/0022-1694\(70\)90255-6](https://doi.org/10.1016/0022-1694(70)90255-6), 1970.
- 651 Newman, A. J., Mizukami, N., Clark, M. P., Wood, A. W., Nijssen, B., Nearing, G., Newman, A. J., Mizukami, N., Clark, M.
652 P., Wood, A. W., Nijssen, B., and Nearing, G.: Benchmarking of a Physically Based Hydrologic Model, *Journal of*
653 *Hydrometeorology*, 18, 2215–2225, <https://doi.org/10/gbwr9s>, 2017.
- 654 Niu, J., Shen, C., Chambers, J., Melack, J. M., and Riley, W. J.: Interannual variation in hydrologic budgets in an Amazonian
655 watershed with a coupled subsurface - land surface process model, *Journal of Hydrometeorology*, 18, 2597–2617,
656 <https://doi.org/10.1175/JHM-D-17-0108.1>, 2017.
- 657 Paszke, A., Gross, S., Chintala, S., Chanan, G., Yang, E., DeVito, Z., Lin, Z., Desmaison, A., Antiga, L., and Lerer, A.:
658 Automatic differentiation in PyTorch, in: 31st Conference on Neural Information Processing Systems (NIPS 2017), Long
659 Beach, CA, 2017.
- 660 Rahmani, F., Lawson, K., Ouyang, W., Appling, A., Oliver, S., and Shen, C.: Exploring the exceptional performance of a deep
661 learning stream temperature model and the value of streamflow data, *Environ. Res. Lett.*, 16, 024025,
662 <https://doi.org/10.1088/1748-9326/abd501>, 2021.
- 663 Rahmani, F., Appling, A., Feng, D., Lawson, K., and Shen, C.: Identifying structural priors in a hybrid differentiable model
664 for stream water temperature modeling, *Water Resources Research*, 59, e2023WR034420,
665 <https://doi.org/10.1029/2023WR034420>, 2023.

- 666 Reichert, P., Ma, K., Höge, M., Fenicia, F., Baity-Jesi, M., Feng, D., and Shen, C.: Metamorphic testing of machine learning
667 and conceptual hydrologic models, *Hydrol. Earth Syst. Sci.*, 28, 2505–2529, <https://doi.org/10.5194/hess-28-2505-2024>, 2024.
- 668 Running, S., Mu, Q., Zhao, M., and Moreno, A.: MODIS/Terra Net Evapotranspiration Gap-Filled 8-Day L4 Global 500m
669 SIN Grid V061, <https://doi.org/10.5067/MODIS/MOD16A2GF.061>, 2021.
- 670 Saha, G., Rahmani, F., Shen, C., Li, L., and Cibin, R.: A deep learning-based novel approach to generate continuous daily
671 stream nitrate concentration for nitrate data-sparse watersheds, *Science of The Total Environment*, 878, 162930,
672 <https://doi.org/10.1016/j.scitotenv.2023.162930>, 2023.
- 673 Seibert, J. and Vis, M. J. P.: Teaching hydrological modeling with a user-friendly catchment-runoff-model software package,
674 *Hydrology and Earth System Sciences*, 16, 3315–3325, <https://doi.org/10/f22r5x>, 2012.
- 675 Shaw, D. A., Pietroniro, A., and Martz, L. w.: Topographic analysis for the prairie pothole region of Western Canada,
676 *Hydrological Processes*, 27, 3105–3114, <https://doi.org/10.1002/hyp.9409>, 2013.
- 677 Shen, C.: A transdisciplinary review of deep learning research and its relevance for water resources scientists, *Water Resources
678 Research*, 54, 8558–8593, <https://doi.org/10.1029/2018wr022643>, 2018.
- 679 Shen, C., Appling, A. P., Gentine, P., Bandai, T., Gupta, H., Tartakovsky, A., Baity-Jesi, M., Fenicia, F., Kifer, D., Li, L., Liu,
680 X., Ren, W., Zheng, Y., Harman, C. J., Clark, M., Farthing, M., Feng, D., Kumar, P., Aboelyazeed, D., Rahmani, F., Song, Y.,
681 Beck, H. E., Bindas, T., Dwivedi, D., Fang, K., Höge, M., Rackauckas, C., Mohanty, B., Roy, T., Xu, C., and Lawson, K.:
682 Differentiable modelling to unify machine learning and physical models for geosciences, *Nat Rev Earth Environ*, 4, 552–567,
683 <https://doi.org/10.1038/s43017-023-00450-9>, 2023.
- 684 Song, Y., Knoben, W. J. M., Clark, M. P., Feng, D., Lawson, K. E., and Shen, C.: When ancient numerical demons meet
685 physics-informed machine learning: adjoint-based gradients for implicit differentiable modeling, *Hydrology and Earth System
686 Sciences Discussions*, 1–35, <https://doi.org/10.5194/hess-2023-258>, 2023.
- 687 Song, Y., Tsai, W.-P., Gluck, J., Rhoades, A., Zarzycki, C., McCrary, R., Lawson, K., and Shen, C.: LSTM-based data
688 integration to improve snow water equivalent prediction and diagnose error sources, *J. Hydrometeorol.*, 25, 223–237,
689 <https://doi.org/10.1175/JHM-D-22-0220.1>, 2024.
- 690 Tsai, W.-P., Feng, D., Pan, M., Beck, H., Lawson, K., Yang, Y., Liu, J., and Shen, C.: From calibration to parameter learning:
691 Harnessing the scaling effects of big data in geoscientific modeling, *Nat Commun*, 12, 5988, [https://doi.org/10.1038/s41467-
692 021-26107-z](https://doi.org/10.1038/s41467-021-26107-z), 2021.
- 693 Vanderhoof, M. K., Christensen, J. R., and Alexander, L. C.: Patterns and drivers for wetland connections in the Prairie Pothole
694 Region, United States, *Wetlands Ecol Manage*, 25, 275–297, <https://doi.org/10.1007/s11273-016-9516-9>, 2017.
- 695 Veldkamp, T. I. E., Zhao, F., Ward, P. J., Moel, H. de, Aerts, J. C. J. H., Schmied, H. M., Portmann, F. T., Masaki, Y., Pokhrel,
696 Y., Liu, X., Satoh, Y., Gerten, D., Gosling, S. N., Zaherpour, J., and Wada, Y.: Human impact parameterizations in global
697 hydrological models improve estimates of monthly discharges and hydrological extremes: a multi-model validation study,
698 *Environ. Res. Lett.*, 13, 055008, <https://doi.org/10.1088/1748-9326/aab96f>, 2018.
- 699 Werth, S. and Güntner, A.: Calibration analysis for water storage variability of the global hydrological model WGHM,
700 *Hydrology and Earth System Sciences*, 14, 59–78, <https://doi.org/10.5194/hess-14-59-2010>, 2010.

- 701 Wunsch, A., Liesch, T., and Broda, S.: Groundwater level forecasting with artificial neural networks: a comparison of long
702 short-term memory (LSTM), convolutional neural networks (CNNs), and non-linear autoregressive networks with exogenous
703 input (NARX), *Hydrology and Earth System Sciences*, 25, 1671–1687, <https://doi.org/10.5194/hess-25-1671-2021>, 2021.
- 704 Xu, D., Agee, E., Wang, J., and Ivanov, V. Y.: Estimation of Evapotranspiration of Amazon Rainforest Using the Maximum
705 Entropy Production Method, *Geophysical Research Letters*, 46, 1402–1412, <https://doi.org/10.1029/2018GL080907>, 2019.
- 706 Yilmaz, K. K., Gupta, H. V., and Wagener, T.: A process-based diagnostic approach to model evaluation: Application to the
707 NWS distributed hydrologic model, *Water Resources Research*, 44, <https://doi.org/10/fpvsgb>, 2008.
- 708 Zaherpour, J., Gosling, S. N., Mount, N., Schmied, H. M., Veldkamp, T. I. E., Dankers, R., Eisner, S., Gerten, D.,
709 Gudmundsson, L., Haddeland, I., Hanasaki, N., Kim, H., Leng, G., Liu, J., Masaki, Y., Oki, T., Pokhrel, Y., Satoh, Y., Schewe,
710 J., and Wada, Y.: Worldwide evaluation of mean and extreme runoff from six global-scale hydrological models that account
711 for human impacts, *Environ. Res. Lett.*, 13, 065015, <https://doi.org/10.1088/1748-9326/aac547>, 2018.
- 712 Zhao, W. L., Gentine, P., Reichstein, M., Zhang, Y., Zhou, S., Wen, Y., Lin, C., Li, X., and Qiu, G. Y.: Physics-constrained
713 machine learning of evapotranspiration, *Geophysical Research Letters*, 46, 14496–14507,
714 <https://doi.org/10.1029/2019gl085291>, 2019.
- 715 Zhi, W., Feng, D., Tsai, W.-P., Sterle, G., Harpold, A., Shen, C., and Li, L.: From hydrometeorology to river water quality:
716 Can a deep learning model predict dissolved oxygen at the continental scale?, *Environ. Sci. Technol.*, 55, 2357–2368,
717 <https://doi.org/10.1021/acs.est.0c06783>, 2021.

718